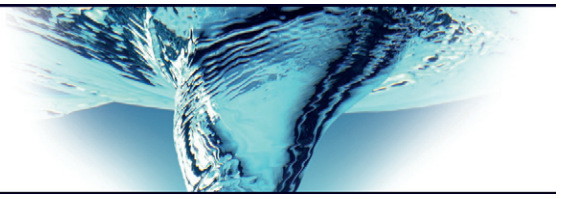
CrossMark

J. Fluid Mech. (2017), *vol.* 823, R3, doi:10.1017/jfm.2017.358



JFM RAPIDS
journals.cambridge.org/rapids

Synthetic jet generation by high-frequency cavitation

Milad Mohammadzadeh[1], Silvestre Roberto Gonzalez-Avila[1], Kun Liu[2], Qi Jie Wang[2] and Claus-Dieter Ohl[1,†]

[1]School of Physical and Mathematical Sciences, Nanyang Technological University, 637371 Singapore, Singapore

[2]School of Electrical and Electronic Engineering, Nanyang Technological University, 639798 Singapore, Singapore

(Received 17 March 2017; revised 10 May 2017; accepted 19 May 2017; first published online 21 June 2017)

Cavitation bubbles are nucleated at a high repetition rate in water by delivering a pulsed laser through a fibre optic. Continuous high-frequency cavitation drives a stream away from the fibre tip. Using high-speed photography and particle image velocimetry, the stream is characterised as a synthetic jet, generated by trains of vortices induced by non-spherical bubble collapse. At low laser power, the bubbles collapse before the arrival of a subsequent laser pulse. Yet, by increasing the laser power, a system of bubbles is formed which leads to complex bubble–bubble interactions. The synthetic jet is observed regardless of the bubble formation regime, demonstrating the stability of the phenomenon. Synthetic jet generation by repetitive bubble collapse extends the well-studied acoustic streaming from small-amplitude bubble oscillations.

Key words: bubble dynamics, cavitation, jets

1. Introduction

Bubbles rarely collapse spherically; they often induce liquid jets at the last stage of their collapse. Rapid microjets are generated when bubbles collapse near rigid (Blake, Taib & Doherty 1986; Vogel, Lauterborn & Timm 1989), elastic (Brujan *et al.* 2001) and free boundaries (Blake, Taib & Doherty 1987), which can penetrate into biological tissue (Kodama & Tomita 2000; Tezel & Mitragotri 2003) or damage hydraulic machinery (Arndt 1981). Jets generated during the collapse of cavitation bubbles have been studied extensively in the literature through experiments, numerical simulations and modelling (Blake & Gibson 1987; Philipp & Lauterborn 1998). During stable bubble oscillations, constant streaming is observed in the liquid surrounding the bubble

† Email address for correspondence: cdohl@ntu.edu.sg

© Cambridge University Press 2017

https://doi.org/10.1017/jfm.2017.358 Published online by Cambridge University Press

(Riley 2001; Tho, Manasseh & Ooi 2007). This microstreaming is comprehensively reported in the literature (Elder 1959; Davidson & Riley 1971; Longuet-Higgins 1998) and applied to poration of biological cells (Marmottant & Hilgenfeldt 2003), selective particle trapping (Rogers & Neild 2011), micromixing (Liu *et al.* 2002) and a variety of applications in lab-on-a-chip devices (Hashmi *et al.* 2012).

While streaming from small-amplitude bubble oscillations is well known, it has received less attention with regard to strongly collapsing cavitation bubbles, i.e. inertial cavitation. These bubbles can be conveniently generated using pulsed lasers (Zwaan *et al.* 2007; Lauterborn & Vogel 2013), shock waves (Apfel 1981; Coleman *et al.* 1987), electrical discharge (Buogo & Cannelli 2002) or localised heating (Azam *et al.* 2013; Li *et al.* 2017). Inertial cavitation is applied in various therapeutic and diagnostic medical procedures (Coussios & Roy 2008), for instance in laser surgeries and tissue ablation, such as ocular surgery (Vogel *et al.* 1986), fragmentation of urinary stones (Vassar *et al.* 1999) and removal of arterial blood clots (Jean & Bende 2003). In most applications involving laser-induced cavitation, the laser repetition period is much larger than the bubble lifetime. Yet, in some applications, such as nanoparticle synthesis, kilohertz or even megahertz laser systems are used (Barcikowski & Compagnini 2013).

In this work, we study the flow induced by steadily generated cavitation bubbles at the cross-over where the repetition period of the cavitation event is of the same order as the lifetime of the bubble. An experimental set-up is presented to generate high-frequency cavitation and visualise the cavitation-induced flow using particle image velocimetry. We characterise the flow field as a synthetic jet and conclude with a model for the bubble formation process.

2. Experimental set-up

To generate cavitation bubbles with high spatial and temporal repeatability, we use a pulsed thulium (Tm) laser (wavelength $\lambda = 1.96$ μm) running at a high repetition rate (Tang *et al.* 2014). The pulsed laser is delivered with a single-mode optical fibre of diameter $d = 250$ μm into a transparent glass container (75 mm × 45 mm × 20 mm) filled with deionised water. The linear absorption of mid-infrared light by the liquid layer adjacent to the fibre tip leads to heating and eventually vaporisation, i.e. generation of a cavitation bubble. The dynamics of this bubble is recorded using a high-speed camera (Photron, FASTCAM SA-X2) with diffused back-illumination from an LED light source (REVOX, SLG-150V). The experimental set-up is shown schematically in figure 1.

The flow field is visualised by seeding water with fluorescent microparticles which are 5 μm in diameter and 1050 kg m^{-3} in density (Thermo Scientific, Fluoro-Max 36-2). Particle fluorescence is excited with a green light sheet from a continuous (CW) laser (Nd:YAG, $\lambda = 532$ nm) focused with a cylindrical lens. The laser sheet illuminates the flow along the fibre axis in the axial and radial directions. Specular reflections are absent in the images due to a filter blocking the laser wavelength. The velocity field is extracted from the microparticle images through standard particle image velocimetry (PIV) analysis using the PIVLab toolbox (Thielicke & Stamhuis 2014).

Before each experiment, the laser pulse duration, τ, and its repetition rate, f, are measured with an InGaAs photodiode (Thorlabs, FGA20) connected to an oscilloscope (LeCroy, WaveRunner 64Xi-A). The average power of the laser, P, is measured with a power meter (Opir, 30A-BB-18), determining the energy of each pulse as $E = P/f$. The

https://doi.org/10.1017/jfm.2017.358 Published online by Cambridge University Press

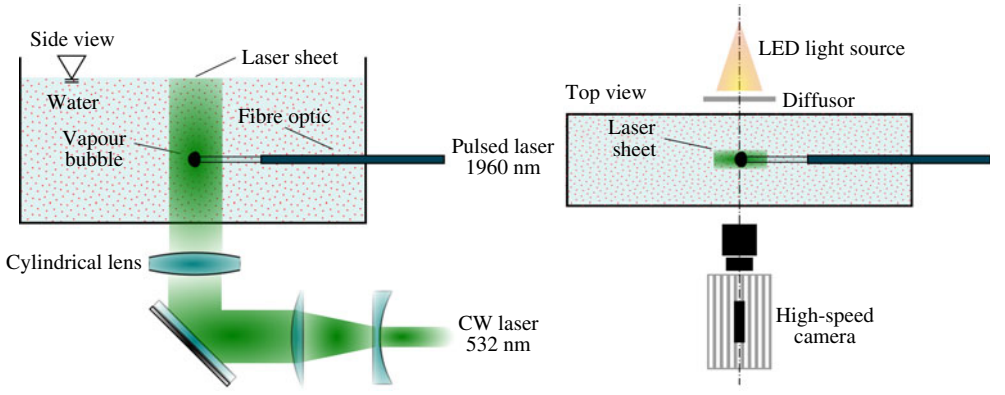


FIGURE 1. Experimental set-up for high-speed photography and particle image velocimetry.

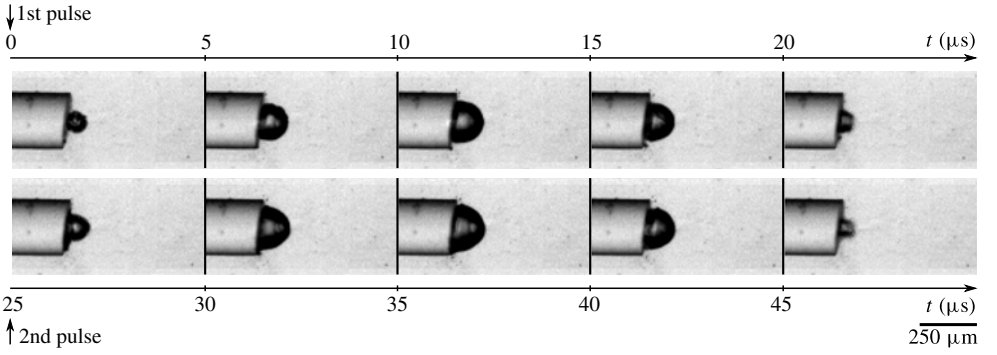


FIGURE 2. High-speed recordings of bubble formation with a high-repetition-rate pulsed laser delivered through an optical fibre. High-frequency cavitation occurs due to linear absorption of the laser energy by the liquid layer adjacent to the fibre tip, forming bubbles that expand and collapse before arrival of the subsequent laser pulse. The laser is operating at $f = 40$ kHz repetition rate and $P = 5$ W average power.

experiments are conducted with three different laser repetition rates, namely $f = 20$, 30 and 40 kHz. The laser power is varied between $P = 2.5$ and 20 W for each repetition rate and the pulse duration τ is between 800 ns and 1 μs.

3. Jet generation by high-frequency cavitation

3.1. *Bubble formation*

Repetitive cavitation is realised with the pulsed laser running at a high repetition rate, as shown in figure 2. Upon delivery of the laser pulse, the liquid layer adjacent to the fibre tip absorbs the pulse energy and undergoes explosive vaporisation, forming an almost hemispherical bubble. This bubble rapidly expands before collapsing under the ambient pressure. At this laser setting, the bubble has already collapsed before an identical bubble is generated with the next laser pulse.

The mechanism of laser-induced cavitation depends on the pulse duration, the irradiation volume and the absorption coefficient of the irradiated medium (Vogel &

https://doi.org/10.1017/jfm.2017.358 Published online by Cambridge University Press

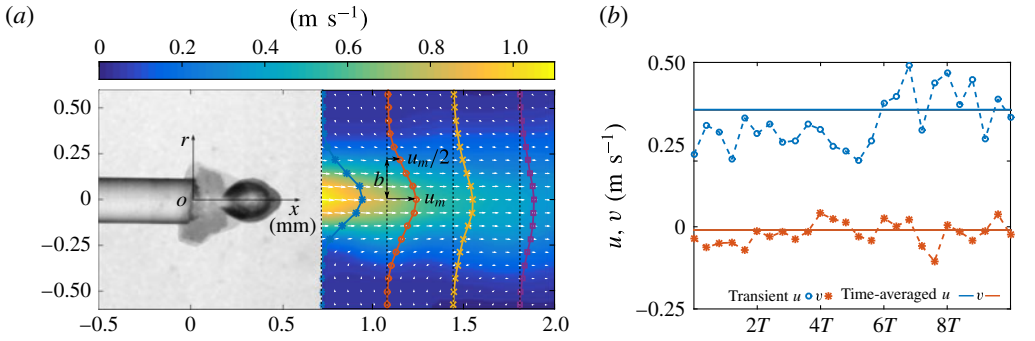


FIGURE 3. (*a*) Time-averaged velocity field induced by high-frequency cavitation visualised by PIV. The time-averaged flow field resembles a continuous free jet directed away from the cavitation site. Semi-transparent photos of the bubble dynamics and the optical fibre are shown to scale. The velocity magnitude, vector field and axial velocity profiles are plotted. (*b*) Transient and time-averaged axial and radial velocity, u and v, at point ($x = 2$ mm, $r = 0$) along the jet over a few periods of the cavitation event $T = f^{-1}$. The laser is operating at a repetition rate of $f = 40$ kHz with an average power of $P = 20$ W.

Venugopalan 2003). In our experiments, the pulse duration τ is longer than the stress relaxation time $\tau_{st} = d/c$, but shorter than the thermal relaxation time $\tau_{th} = d^2/4k$, i.e. $\tau_{st} < \tau < \tau_{th}$. Here, c is the speed of sound and k is the thermal diffusivity in the liquid medium. This condition, known as thermal confinement, means that strong shock waves are not emitted from the irradiation site, yet the temperature in the irradiated volume can increase above the spinodal limit before phase explosion forms a vapour bubble (Frenz *et al.* 1998).

A few seconds after switching on the laser, the bubble formation process becomes highly repeatable. Meanwhile, by increasing the laser power, the bubble may show a different periodicity from the laser pulse. We discuss the effects of laser power and repetition rate on bubble dynamics in § 4, but first we focus on the flow field induced by cavitation in the experiments.

3.2. *Jet characteristics*

Flow field visualisation reveals a stream of particles moving in the axial direction away from the fibre tip, as seen in supplementary movie 1 available at https://doi.org/10.1017/jfm.2017.358. Close to the fibre tip, the motion is complex, with particles following the oscillatory bubble expansion and collapse. Particles that are away from the fibre tip in the radial direction become gradually attracted towards the fibre axis, accelerating as they approach the tip. Since the flow varies with time, we resort to analysing the time-averaged flow field to characterise the stream. Due to imaging limitations, we analyse the flow starting from a distance of approximately three fibre diameters from the fibre tip.

Figure 3(*a*) shows the time-averaged flow field, while the time-variant velocity at a sample point along the stream is plotted in figure 3(*b*). On the left of figure 3(*a*), snapshots of the bubble and fibre tip are overlaid to scale. The time-averaged velocity field reveals a pronounced jet directed away from the fibre tip with an almost axisymmetric flow field, as indicated by the radial profiles of the axial velocity $u(x, r)$.

https://doi.org/10.1017/jfm.2017.358 Published online by Cambridge University Press

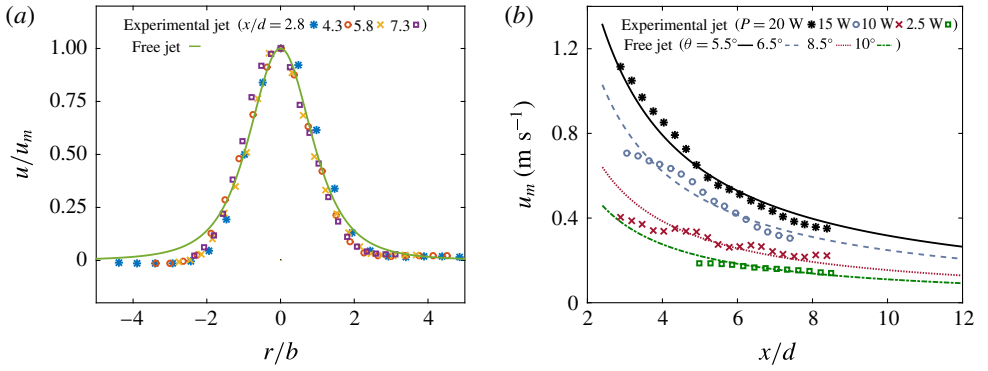


FIGURE 4. (*a*) Comparison between the self-similar velocity profile of the continuous free jet (solid line) and the time-averaged cavitation-induced jet (symbols). The laser is operating at $f = 40$ kHz and $P = 20$ W. (*b*) Decay of the jet centreline velocity $u_m = u(x, r = 0)$ for free jets (lines) and cavitation-induced jets (symbols). The origin of the free jets is fixed at the fibre tip and the cone angles are obtained from the experimental data.

The velocity profiles demonstrate that the jet expands as it travels away from the cavitation site. While the cavitation-induced jet is transient, the time-averaged flow field resembles a steady jet (Rajaratnam 1976).

To study this flow field in more detail, we compare the cavitation-induced jet with a free axisymmetric jet without swirl. Sufficiently far from the origin, free jets are characterised by a self-similar velocity profile (Schlichting & Gersten 2017); i.e. their axial velocity is $u/u_m = (1 + \eta^2)^{-2}$, where $\eta = \sigma r/x$ is the similarity variable. Here, σ is a constant and u_m is the axial velocity along the jet centreline, i.e. $u(x, r = 0)$. This similarity solution is plotted in figure 4(*a*) with a solid line, i.e. $u/u_m = f(r/b)$. Here, b represents the jet half-width, where the velocity drops to half of the jet centreline velocity u_m, marked in figure 3(*a*). The jet half-width grows linearly along free jets, i.e. $b \propto x$ (Rajaratnam 1976). The time-averaged velocity profile of the cavitation-induced jet in the experiments matches well with the similarity solution for the axisymmetric free jet, particularly close to the jet centreline, $r = 0$. This is shown in figure 4(*a*), where the symbols represent various cross-sections along the flow marked in figure 3(*a*).

A second prominent property of the similarity solution for a free jet is that the centreline velocity drops as $u_m \propto 1/x$ along the jet (Rajaratnam 1976). We put this property to test for jets generated at different laser powers. By placing the origin of the free jet at the centre of the fibre tip and estimating the cone angle of the jet from the experimental data (Schlichting & Gersten 2017), agreement is obtained for the time-averaged velocity drop $u_m(x)$ along cavitation-induced jets. The agreement closer to the tip improves as the laser power increases. Additionally, figure 4(*b*) reveals that with increasing laser power, the cone angle of the continuous jet decreases; i.e. a stronger more slender jet is produced.

3.3. *Mechanism of synthetic jet generation*

Despite the transient cavitation activity at the fibre tip, a time-averaged jet is produced which resembles an axisymmetric free jet. Looking in closer detail at the bubble

https://doi.org/10.1017/jfm.2017.358 Published online by Cambridge University Press

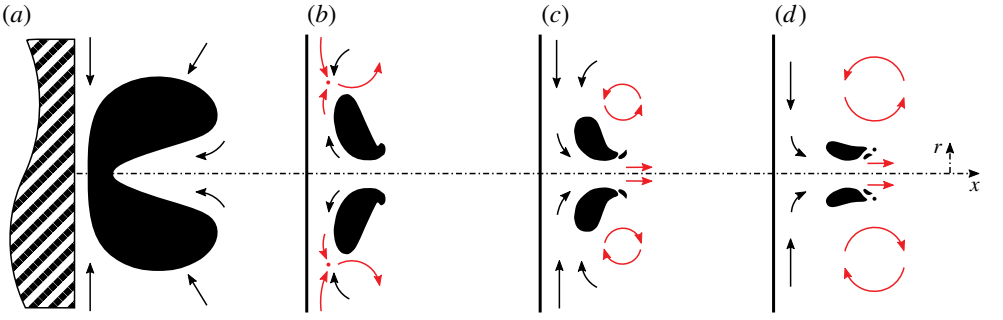


FIGURE 5. Schematic illustration of a collapsing bubble that directs the flow away from a rigid boundary. Important flow features are marked in red. (*a*) The collapsing bubble generates a rapid microjet towards the boundary. (*b*) After jet impingement, remnants of the microjet compete with a strong radial inflow, forming an annular stagnation ring and a rebounding splash. (*c*) The splash develops into a toroidal vortex. (*d*) The vortex moves away from the boundary and carries the bubble fragments along the axis of symmetry.

dynamics, shown in figure 2, the cavitation bubble expands with its centre of mass moving away from the fibre tip, and during shrinkage moves towards it. During the collapse of a translating cavitation bubble, a re-entrant microjet is generated in the direction of its motion (Blake *et al.* 1986; Zhang, Duncan & Chahine 1993; Zhang & Duncan 1994), which is towards the fibre tip. Yet, we observe a large-scale flow away from the fibre. The mechanism that drives the flow away from the boundary may be explained by the repelling motion of a stable vortex ring. The course of events leading to the generation of this vortex ring after each cavitation event is schematically illustrated in figure 5. After jet impingement on a boundary due to the collapse of a sufficiently close bubble, the re-entrant jet competes with the radial inflow as the bubble is still shrinking. This leads to the formation of an annular stagnation ring. We speculate that the radial inflow is reflected away from the boundary as a splash (Tong *et al.* 1999; Brujan *et al.* 2002). This flow may then close into a vortex ring which moves away from the fibre tip due to its rotation direction. An experimental visualisation of a similar process is reported by Reuter *et al.* (2017) in front of a large rigid boundary.

Streaming driven by trains of vortices has been comprehensively studied in the literature under the title of synthetic jets (Glezer & Amitay 2002). Synthetic jets are usually generated by alternating suction and ejection of fluid across an orifice (Mallinson, Reizes & Hong 2001). In contrast to continuous jets, synthetic jets are produced without injecting mass into the system. These jets work merely due to transfer of momentum, typically by oscillations of a membrane or diaphragm (Smith & Swift 2003). In the current set-up, high-frequency cavitation provides the momentum for a synthetic jet, generating a stream with zero net mass flux. As the jet travels away from the cavitation site, it eventually spreads out, directing streamlines back to the cavitation site which complete a loop and feed the jet. In addition to pulsed lasers, spark generators and microheaters may be used to generate cavitation-based synthetic jets.

https://doi.org/10.1017/jfm.2017.358 Published online by Cambridge University Press

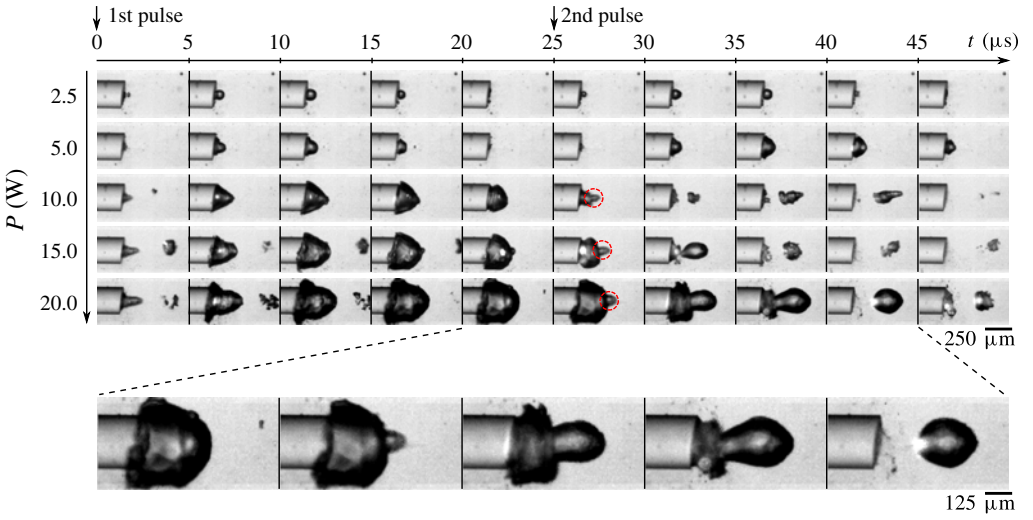


FIGURE 6. The effect of increasing laser power on bubble formation with a high-repetition-rate pulsed laser operating at $f = 40$ kHz. By increasing the average laser power from top to bottom, the bubble size increases. Above a certain threshold, the formation of a secondary bubble at the tip of the initial hemispherical bubble is observed. This occurs when the lifetime of the first bubble is larger than the period of pulse repetition.

4. Bubble formation and dynamics

4.1. *Secondary bubble formation*

An increase in the energy input to the system not only strengthens the jet, as shown in figure 4(*b*), but also affects the bubble dynamics (Mohammadzadeh *et al.* 2016). Figure 6 shows five series of images of bubble formation and collapse, where the laser power is increased from $P = 2.5$ to 20 W. The results are shown at a repetition rate of $f = 40$ kHz, but identical bubble dynamics are observed at other tested repetition rates. As is shown in the two top rows of figure 6, at low laser power, a small bubble forms and collapses on the tip before the next laser pulse arrives. An increase in the laser power may drastically affect the bubble dynamics, as shown in the bottom three rows of figure 6. If the pulse energy is sufficiently high, the initial bubble does not collapse when the next pulse arrives. This allows the laser pulse to be transmitted through the shrinking bubble, leading to vaporisation of the liquid at its distal end and formation of a secondary bubble. A close-up of this process is shown at the bottom of figure 6. While the first bubble shrinks and collapses on the fibre tip, the second one expands and moves away. This repelling motion, caused by out-of-phase oscillation of the two bubbles, may affect the jet generation mechanism (Tomita, Sato & Shima 1994; Yuan, Sankin & Zhong 2011; Han *et al.* 2015). Small vapour fragments of the secondary bubble are still visible when the next laser pulse is absorbed by the liquid layer adjacent to the fibre tip, restarting the bubble formation cycle. As seen in supplementary movie 2, this double-bubble system, composed of the initial and secondary bubbles, follows a cycle with twice the period of pulse repetition.

https://doi.org/10.1017/jfm.2017.358 Published online by Cambridge University Press

4.2. *Model for bubble growth*

Here, we develop a model to predict the growth of the vapour bubble to its maximum size based on the laser pulse energy. Under thermal confinement, the laser pulse heats up the liquid over the fibre core to the critical point, where there is no phase boundary between the liquid and the vapour (Cleary 1977). Thus, we start from an initial nucleus at the critical state where the pressure and density are $p_i = 218$ atm and $\rho_i = 322$ kg m^{-3}. The growth dynamics is modelled as a hemispherical cavitation bubble undergoing explosive expansion without heat transfer. Therefore, the evolution of the bubble radius, $R(t)$, can be modelled with the Rayleigh–Plesset equation (Brennen 2013),

$$R\ddot{R} + \frac{3}{2}\dot{R}^2 = \frac{-p_\infty + p_g}{\rho_l} - \frac{4\nu_l \dot{R}}{R} - \frac{2\sigma}{\rho_l R}, \tag{4.1}$$

where dots denote derivatives with respect to time. The material properties are the density of the liquid, $\rho_l = 10^3$ kg m^{-3}, the kinematic viscosity of the liquid, $\nu_l = 10^{-6}$ m^2 s^{-1}, and the surface tension, $\sigma = 0.072$ N m^{-1}. With negligible heat transfer and phase change over the bubble interface due to its rapid growth, the pressure in the bubble, p_g, evolves adiabatically, i.e. $p_g = p_i(R_i/R)^{3\gamma}$, where $\gamma = 4/3$ is the adiabatic exponent. The bubble expansion is countered by the ambient pressure, $p_\infty = 1$ atm.

If we have the initial state of the vapour, the initial bubble radius R_i can be determined from the absorbed energy of the laser pulse E_{abs}, which is used to raise the state of the liquid to the critical point. The specific energy, i.e. energy per unit mass of the liquid, needed for this change of state is $h = 2.84 \times 10^3$ kJ kg^{-1}. To calculate this, we use a thermodynamic path in which water is first heated up isobarically from ambient conditions to 373 K, phase change from liquid to vapour occurs at 373 K, the vapour is heated up under ambient pressure to the critical temperature of 647 K and finally the steam at critical temperature is pressurised isothermally to the critical pressure of 218 atm (Gerstman *et al.* 1995). Assuming that the initial vapour bubble at the fibre tip has a hemispherical shape, we can write the energy balance as

$$\tfrac{2}{3}\pi R_i^3 \rho_i h = E_{abs}. \tag{4.2}$$

In the current experiments, the liquid absorbs the laser energy through linear absorption, i.e. $E_{abs} = \alpha H_0 V_{irr}$, where α is the linear absorption coefficient, H_0 is the laser fluence and V_{irr} is the irradiated volume. For water, the absorption coefficient at $\lambda = 1.96$ μm is $\alpha \approx 100$ cm^{-1}. Using the fibre core radius $l_i = 25$ μm as the irradiation length scale, the laser fluence H_0 is $E/\pi l_i^2$. Approximation of the irradiated volume as a hemisphere, $V_{irr} = 2/3\pi l_i^3$, results in an absorbed energy of $E_{abs} = 2/3\alpha l_i E$, which combined with (4.2) gives an estimation for the initial bubble radius,

$$R_i^3 = \frac{\alpha l_i}{\pi \rho_i h} E. \tag{4.3}$$

Inserting the laser pulse energy from the experiments (0.0625 mJ $< E < 1$ mJ), we use the initial bubble radius R_i from (4.3) as the initial condition for the cavitation model in (4.1). After numerical integration, we obtain the maximum bubble radius R_{max}, which is compared with the experiments in figure 7(*a*). The maximum bubble radii from the experiments are estimated by averaging the bubble extensions in the radial and axial directions over multiple cycles. In general, the model agrees well with the experiments, despite some discrepancy at the lowest pulse energy. This model also allows us to determine the laser settings that lead to secondary bubble

https://doi.org/10.1017/jfm.2017.358 Published online by Cambridge University Press

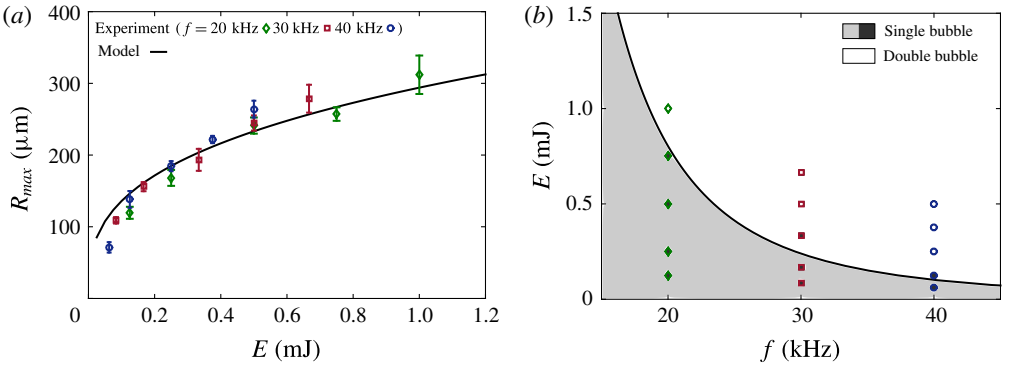


FIGURE 7. (*a*) Maximum bubble radius R_{max} as a function of the laser pulse energy E. The experimental results are compared with the model presented in § 4.2 for three different laser repetition rates. (*b*) The laser pulse energy E needed for secondary bubble formation as a function of the pulse repetition rate f. The grey colour marks the region and experimental data with only hemispherical bubble formation, and white denotes the formation of secondary bubbles.

formation. As shown in figure 6, a secondary bubble forms when the initial bubble is large enough such that it has not collapsed when the next laser pulse arrives. This condition can be quantified as $2t_c > 1/f$. Here, t_c is the Rayleigh collapse time of a bubble, which is known to increase linearly with the maximum bubble radius, i.e. $t_c = 0.915\sqrt{(\rho_l/p_\infty)}R_{max}$ (Brennen 2013). For a given laser repetition rate f, the pulse energy E that is sufficiently large for secondary bubble formation is calculated from the Rayleigh–Plesset model and plotted as a function of the repetition rate f in figure 7(*b*). Overall, we find excellent agreement with the cavitation regime observed experimentally.

5. Discussion and conclusion

Synthetic jets are advantageous in various flow control applications as they eliminate the need to inject mass into the system. For instance, synthetic jet actuators can be mounted on an object to affect the hydrodynamic forces by interacting with the cross-flow over the object (Glezer & Amitay 2002). Slow synthetic jets of millimetres per second velocity have been produced by oscillating sessile bubbles through the control of surface wetting (Ko, Lee & Kang 2009). In this article, we present a unique synthetic jet in which high-frequency cavitation provides the momentum for a jet of up to 1.2 m s^{-1} in velocity, which speeds up with increasing laser power. The time-averaged velocity field for this synthetic jet agrees well with the self-similar velocity profile of the axisymmetric free jet, particularly along the axis and for stronger jets. The strength of a free jet is inversely proportional to its cone angle and is determined by its kinematic momentum K_a (Schlichting & Gersten 2017). We speculate that for the cavitation-induced jet, $K_a \propto U_v^2 R_{max}^2$, where U_v is the velocity of the collapse-induced toroidal vortex as it travels away from a rigid boundary. The motion of this vortex core depends on the bubble size and its distance from the boundary (Reuter *et al.* 2017).

Synthetic jet generation from cavitation bubbles could be advantageous for flow actuation in microfluidics by eliminating the need for a mass source. By directing the

https://doi.org/10.1017/jfm.2017.358 Published online by Cambridge University Press

flow, these jets can also reduce the need for microchannel fabrication (Marmottant *et al.* 2006). Additionally, streaming from cavitation bubbles is relevant in medical applications, since these bubbles play an important role in laser surgeries by acting as transmission channels to ablation targets (Vogel & Venugopalan 2003). In particular, bubbles formed with mid-infrared lasers, such as the thulium laser used in the current study, are known to significantly affect the mass removal efficiency and resolution (Pratisto *et al.* 1996) and motion of the ablation target (Kang *et al.* 2006; Mohammadzadeh, Mercado & Ohl 2015). We have found the strength of the synthetic jet to be proportional to the laser power, which in turn determines the bubble size. A model is presented to estimate the bubble size and determine the energy needed for secondary bubble formation, a cavitation regime that allows the generation of non-spherical bubbles with short energy impulses and leads to strong bubble–bubble interactions.

Acknowledgement

The authors gratefully acknowledge the financial support from Nanyang Technological University, Singapore.

Supplementary movies

Supplementary movies are available at https://doi.org/10.1017/jfm.2017.358.

References

APFEL, R. E. 1981 Acoustic cavitation prediction. *J. Acoust. Soc. Am.* **69** (6), 1624–1633.

ARNDT, R. E. A. 1981 Cavitation in fluid machinery and hydraulic structures. *Annu. Rev. Fluid Mech.* **13** (1), 273–326.

AZAM, F. I., KARRI, B., OHL, S.-W., KLASEBOER, E. & KHOO, B. C. 2013 Dynamics of an oscillating bubble in a narrow gap. *Phys. Rev.* E **88** (4), 043006.

BARCIKOWSKI, S. & COMPAGNINI, G. 2013 Advanced nanoparticle generation and excitation by lasers in liquids. *Phys. Chem. Chem. Phys.* **15** (9), 3022–3026.

BLAKE, J. R. & GIBSON, D. C. 1987 Cavitation bubbles near boundaries. *Annu. Rev. Fluid Mech.* **19** (1), 99–123.

BLAKE, J. R., TAIB, B. B. & DOHERTY, G. 1986 Transient cavities near boundaries. Part 1. Rigid boundary. *J. Fluid Mech.* **170**, 479–497.

BLAKE, J. R., TAIB, B. B. & DOHERTY, G. 1987 Transient cavities near boundaries. Part 2. Free surface. *J. Fluid Mech.* **181**, 197–212.

BRENNEN, C. E. 2013 *Cavitation and Bubble Dynamics*. Cambridge University Press.

BRUJAN, E. A., KEEN, G. S., VOGEL, A. & BLAKE, J. R. 2002 The final stage of the collapse of a cavitation bubble close to a rigid boundary. *Phys. Fluids* **14** (1), 85–92.

BRUJAN, E.-A., NAHEN, K., SCHMIDT, P. & VOGEL, A. 2001 Dynamics of laser-induced cavitation bubbles near an elastic boundary. *J. Fluid Mech.* **433**, 251–281.

BUOGO, S. & CANNELLI, G. B. 2002 Implosion of an underwater spark-generated bubble and acoustic energy evaluation using the Rayleigh model. *J. Acoust. Soc. Am.* **111** (6), 2594–2600.

CLEARY, S. F. 1977 Laser pulses and the generation of acoustic transients in biological material. In *Laser Applications in Medicine and Biology*, pp. 175–219. Springer.

COLEMAN, A. J., SAUNDERS, J. E., CRUM, L. A. & DYSON, M. 1987 Acoustic cavitation generated by an extracorporeal shockwave lithotripter. *Ultrasound Med. Biol.* **13** (2), 69–76.

COUSSIOS, C. C. & ROY, R. A. 2008 Applications of acoustics and cavitation to noninvasive therapy and drug delivery. *Annu. Rev. Fluid Mech.* **40**, 395–420.

DAVIDSON, B. J. & RILEY, N. 1971 Cavitation microstreaming. *J. Sound Vib.* **15** (2), 217–233.

ELDER, S. A. 1959 Cavitation microstreaming. *J. Acoust. Soc. Am.* **31** (1), 54–64.

https://doi.org/10.1017/jfm.2017.358 Published online by Cambridge University Press

FRENZ, M., KÖNZ, F., PRATISTO, H., WEBER, H. P., SILENOK, A. S. & KONOV, V. I. 1998 Starting mechanisms and dynamics of bubble formation induced by a Ho:yttrium aluminum garnet laser in water. *J. Appl. Phys.* **84** (11), 5905–5912.

GERSTMAN, B. S., THOMPSON, C. R., JACQUES, S. L. & ROGERS, M. E. 1995 Laser-induced bubble formation in the retina. In *Photonics West'95*, pp. 60–71. International Society for Optics and Photonics.

GLEZER, A. & AMITAY, M. 2002 Synthetic jets. *Annu. Rev. Fluid Mech.* **34** (1), 503–529.

HAN, B., KÖHLER, K., JUNGNICKEL, K., METTIN, R., LAUTERBORN, W. & VOGEL, A. 2015 Dynamics of laser-induced bubble pairs. *J. Fluid Mech.* **771**, 706–742.

HASHMI, A., YU, G., REILLY-COLLETTE, M., HEIMAN, G. & XU, J. 2012 Oscillating bubbles: a versatile tool for lab on a chip applications. *Lab on a Chip* **12** (21), 4216–4227.

JEAN, B. & BENDE, T. 2003 Mid-IR laser applications in medicine. In *Solid-State Mid-Infrared Laser Sources*, pp. 530–565. Springer.

KANG, H. W., LEE, H., TEICHMAN, J. M., OH, J., KIM, J. & WELCH, A. J. 2006 Dependence of calculus retropulsion on pulse duration during Ho:YAG laser lithotripsy. *Laser Surg. Med.* **38** (8), 762–772.

KO, S. H., LEE, S. J. & KANG, K. H. 2009 A synthetic jet produced by electrowetting-driven bubble oscillations in aqueous solution. *Appl. Phys. Lett.* **94** (19), 194102.

KODAMA, T. & TOMITA, Y. 2000 Cavitation bubble behavior and bubble–shock wave interaction near a gelatin surface as a study of in vivo bubble dynamics. *Appl. Phys.* B **70** (1), 139–149.

LAUTERBORN, W. & VOGEL, A. 2013 Shock wave emission by laser generated bubbles. In *Bubble Dynamics and Shock Waves*, pp. 67–103. Springer.

LI, F., GONZALEZ-AVILA, S. R., NGUYEN, D. M. & OHL, C.-D. 2017 Oscillate boiling from microheaters. *Phys. Rev. Fluids* **2** (1), 014007.

LIU, R. H., YANG, J., PINDERA, M. Z., ATHAVALE, M. & GRODZINSKI, P. 2002 Bubble-induced acoustic micromixing. *Lab on a Chip* **2** (3), 151–157.

LONGUET-HIGGINS, M. S. 1998 *Viscous Streaming from an Oscillating Spherical Bubble*, vol. 454, pp. 725–742. The Royal Society.

MALLINSON, S. G., REIZES, J. A. & HONG, G. 2001 An experimental and numerical study of synthetic jet flow. *Aeronaut. J.* **105** (1043), 41–49.

MARMOTTANT, P. & HILGENFELDT, S. 2003 Controlled vesicle deformation and lysis by single oscillating bubbles. *Nature* **423** (6936), 153–156.

MARMOTTANT, P., RAVEN, J. P., GARDENIERS, H. J. G. E., BOMER, J. G. & HILGENFELDT, S. 2006 Microfluidics with ultrasound-driven bubbles. *J. Fluid Mech.* **568**, 109–118.

MOHAMMADZADEH, M., CHAN, W., GONZALEZ-AVILA, S. R., LIU, K., WANG, Q. J. & OHL, C.-D. 2016 Bubble formation with a high repetition rate pulsed Tm laser. In *Proceedings of The 20th Australasian Fluid Mechanics Conference* ISBN: 978-1-74052-377-6 http://people.eng.unimelb.edu.au/imarusic/proceedings/20%20AFMC%20TOC.htm.

MOHAMMADZADEH, M., MERCADO, J. M. & OHL, C. D. 2015 Bubble dynamics in laser lithotripsy. In *Journal of Physics Conference Series*, vol. 656, p. 012004. IOP Publishing.

PHILIPP, A. & LAUTERBORN, W. 1998 Cavitation erosion by single laser-produced bubbles. *J. Fluid Mech.* **361**, 75–116.

PRATISTO, H., FRENZ, M., ITH, M., ALTERMATT, H. J., JANSEN, E. D. & WEBER, H. P. 1996 Combination of fiber-guided pulsed erbium and holmium laser radiation for tissue ablation under water. *Appl. Opt.* **35** (19), 3328–3337.

RAJARATNAM, N. 1976 *Turbulent Jets*, vol. 5. Elsevier.

REUTER, F., GONZALEZ-AVILA, S. R., METTIN, R. & OHL, C.-D. 2017 Flow fields and vortex dynamics of bubbles collapsing near a solid boundary. *Phys. Rev. Fluids* **2**, 064202.

RILEY, N. 2001 Steady streaming. *Annu. Rev. Fluid Mech.* **33** (1), 43–65.

ROGERS, P. & NEILD, A. 2011 Selective particle trapping using an oscillating microbubble. *Lab on a Chip* **11** (21), 3710–3715.

SCHLICHTING, H. & GERSTEN, K. 2017 *Boundary-Layer Theory*. Springer.

SMITH, B. L. & SWIFT, G. W. 2003 A comparison between synthetic jets and continuous jets. *Exp. Fluids* **34** (4), 467–472.

https://doi.org/10.1017/jfm.2017.358 Published online by Cambridge University Press

TANG, Y., LI, X., YAN, Z., YU, X., ZHANG, Y. & WANG, Q. J. 2014 50-W 2-μm nanosecond all-fiber-based thulium-doped fiber amplifier. *IEEE J. Sel. Top. Quant.* **20** (5), 537–543.

TEZEL, A. & MITRAGOTRI, S. 2003 Interactions of inertial cavitation bubbles with stratum corneum lipid bilayers during low-frequency sonophoresis. *Biophys. J.* **85** (6), 3502–3512.

THIELICKE, W. & STAMHUIS, E. 2014 PIVLab – towards user-friendly, affordable and accurate digital particle image velocimetry in MATLAB. *J. Open Res. Softw.* **2** (1), e30.

THO, P., MANASSEH, R. & OOI, A. 2007 Cavitation microstreaming patterns in single and multiple bubble systems. *J. Fluid Mech.* **576**, 191–233.

TOMITA, Y., SATO, K. & SHIMA, A. 1994 Interaction of two laser-produced cavitation bubbles near boundaries. In *Bubble Dynamics and Interface Phenomena*, pp. 33–45. Springer.

TONG, R. P., SCHIFFERS, W. P., SHAW, S. J., BLAKE, J. R. & EMMONY, D. C. 1999 The role of splashing in the collapse of a laser-generated cavity near a rigid boundary. *J. Fluid Mech.* **380**, 339–361.

VASSAR, G. J., CHAN, K. F., TEICHMAN, J. M. H., GLICKMAN, R. D., WEINTRAUB, S. T., PFEFER, T. J. & WELCH, A. J. 1999 Holmium:YAG lithotripsy: photothermal mechanism. *J. Endourol.* **13** (3), 181–190.

VOGEL, A., HENTSCHEL, W., HOLZFUSS, J. & LAUTERBORN, W. 1986 Cavitation bubble dynamics and acoustic transient generation in ocular surgery with pulsed neodymium:YAG lasers. *Ophthalmology* **93** (10), 1259–1269.

VOGEL, A., LAUTERBORN, W. & TIMM, R. 1989 Optical and acoustic investigations of the dynamics of laser-produced cavitation bubbles near a solid boundary. *J. Fluid Mech.* **206**, 299–338.

VOGEL, A. & VENUGOPALAN, V. 2003 Mechanisms of pulsed laser ablation of biological tissues. *Chem. Rev.* **103** (2), 577–644.

YUAN, F., SANKIN, G. & ZHONG, P. 2011 Dynamics of tandem bubble interaction in a microfluidic channel. *J. Acoust. Soc. Am.* **130** (5), 3339–3346.

ZHANG, S. & DUNCAN, J. H. 1994 On the nonspherical collapse and rebound of a cavitation bubble. *Phys. Fluids* **6** (7), 2352–2362.

ZHANG, S., DUNCAN, J. H. & CHAHINE, G. L. 1993 The final stage of the collapse of a cavitation bubble near a rigid wall. *J. Fluid Mech.* **257**, 147–181.

ZWAAN, E., LE GAC, S., TSUJI, K. & OHL, C.-D. 2007 Controlled cavitation in microfluidic systems. *Phys. Rev. Lett.* **98**, 254501.

https://doi.org/10.1017/jfm.2017.358 Published online by Cambridge University Press